

# Seismic, geologic, geomechanics, and dynamic constraints in flow models of unconventional fractured reservoirs: Example from a south Texas field



Reinaldo J. Michelena<sup>1</sup>, James R. Gilman<sup>1</sup>, and Christopher K. Zahm<sup>2</sup>

<https://doi.org/10.1190/tle38020116.1>

## Abstract

We present a workflow to build permeability models for flow simulation in unconventional naturally fractured reservoirs constrained by 3D seismic, geologic data and concepts, geomechanics observations, and dynamic data. Joints and faults are modeled separately to account for their differences in scale and flow properties. Seismic-derived orientation statistics are compared against orientations from outcrops and microseismic data to assess their validity and consistency across multiple scales. We show the impact of natural fractures and stress orientation in the flow and variability of the pressure field around producing wells in an unconventional reservoir from south Texas. Such variability can have a significant impact on well interference and optimal well spacing.

## Introduction

Fluid flow in unconventional naturally fractured reservoirs depends on the interaction of complex parameters such as matrix properties, natural fracture properties, fluid saturations and pressures, fluid pressure-volume behavior, stimulation parameters, and local stress conditions. Flow simulation is a tool that can help us understand these complex interactions, calibrate the concepts incorporated into geologic and dynamic models, understand the nature of the production decline, and make production forecasts.

If the complexities in the development of unconventional reservoirs are addressed by making simplistic assumptions about some of the parameters, we may reach conclusions that can lead to erroneous decisions regarding the exploitation of the resource. Even though significant advances have been made in the area of flow simulation of unconventional reservoirs to account for their unique complexities of intrinsic flow mechanisms (e.g., Yan et al., 2013; Farah, 2016), the homogeneity of rock properties is still a common assumption in field scale studies. Homogeneous matrix and fracture properties result in biwing symmetric stimulated fracture areas that when used to understand depletion in unconventional reservoirs may lead to erroneous conclusions regarding well communication, drainage zones, and bypassed oil, which impact infill drilling and ultimate recovery.

For more than three decades, seismic data have been used to help in the construction of rock property models in conventional reservoirs. In unconventional reservoirs, however, such extensive experience has not been mimicked, and studies that incorporate seismic data into reservoir models that are used for flow simulation are still uncommon in public literature. Such studies typically tend to emphasize the distribution of matrix properties without considering possible variability and influence of natural fracture properties

(e.g., Torres-Parada et al., 2018), or they focus on a single well and the specifics of the completion (e.g., Cipolla et al., 2011).

In this paper, we show an example of the application of a workflow that uses seismic data to constrain the matrix and fracture components of a detailed flow simulation model in a south Texas unconventional reservoir. Since characterization and modeling of the matrix is described in a separate paper (Michelena et al., 2017), we focus this paper on the characterization and modeling of the natural fractures component of the model, the use of the matrix-fracture model for flow simulation, and what kind of insight flow simulation results can provide to understand the nature of depletion. Understanding of natural fractures in unconventional reservoirs is important because natural fractures may enhance fluid flow from the matrix into the wellbore and play an important role in hydraulic fracture (HF) stimulation.

We start by describing a workflow to extract, map, and calibrate natural fractures from 3D seismic data that are used to constrain fracture modeling and flow simulation models. Extensional fractures (joints) and shear fractures (faults) are modeled separately to account for their different sizes and flow properties in the flow simulator and to assess their relative importance when calibrating with production data. Once the seismic-derived fracture information has been properly calibrated with outcrop and microseismic data, we briefly explain how to upscale the fracture models for effective permeability by considering the effect of current-day earth stress. We then illustrate the dynamically modeled heterogeneity in the pressure field that results after incorporating all the spatial variability in matrix and natural fractures. With the use of a fast graphic processing unit (GPU)-based dual-permeability flow simulation, we are able to preserve details of the model that not only behave similar to commonly used single-well local grid refinement (LGR) methods for early time pressure response modeling but also allow long-term tracking of pressure change over large distances. The result is a significantly heterogeneous pressure field that may impact optimal infill drilling and well-spacing decisions.

## Interval of interest

The unconventional reservoir analyzed in this study is located in south Texas (Figure 1a). One pilot well and eight horizontal wells have been drilled in the area of interest for flow simulation that covers approximately 3.6 mi<sup>2</sup> (Figure 1b). The interval of interest is approximately 200 ft thick and consists mostly of carbonate facies (porous packstone, porous mudstone, and tight carbonate) with a small proportion of kerogen-rich clay layers. Most clay layers are located in the deeper portion of the interval and are not a target

<sup>1</sup>Reservoir.com Inc., Littleton, Colorado, USA. E-mail: michelena@ireservoir.com; gilman@ireservoir.com.

<sup>2</sup>Bureau of Economic Geology, University of Texas at Austin, Austin, Texas, USA. E-mail: chris.zahm@beg.utexas.edu.

for horizontal drilling in the area. Facies were defined by petrophysical analyses in the pilot well and calibrated with core data (not shown). Calcite is the dominant mineral, and experience in the area indicates that brittleness is proportional to calcite content and decreases with clay content.

Outcrop analogs can be an important data source as the spatial arrangements of facies and fractures can be explored. Figure 2 shows an outcrop of the Late Cretaceous Boquillas Formation, which is considered a good analog for the formation of interest in this study. Natural fractures of different sizes and origins (joints and faults) can be observed in the exposure. Notice the differences between the two regarding their number, relation to rock properties of individual layers, and vertical connectivity. Both types of fractures are below seismic resolution but are expected to have significantly different flow properties.

The seismic data used in this study are part of a large merge of several 3D seismic surveys that cover an area of approximately 280 mi<sup>2</sup>. The details of the characterization and seismic constrained modeling of matrix properties in the interval of interest can be found in Michelena et al. (2017).

### Fracture modeling workflow

Fluid flow in natural fractures depends on how the fractures originated (e.g., extension versus shear), their geometry, spatial distribution, and quality. Fracture quality (i.e., flow capacity potential) is determined by current stress conditions and diagenetic alterations that may have occurred to the fractures after formation (National Research Council, 1996).

Our fracture modeling workflow emphasizes the parameters that control fluid flow (geologic origin of the fractures, distribution and geometry, and fracture quality). Joints (or bed-bound fractures) and small faults (sometimes referred to as through-going fractures) are modeled separately to be able to account for their differences in flow properties and test their relative importance in the flow simulator. Although joints (controlled by rock properties, mechanical stratigraphy, bed thickness, and stress state) may have diminished apertures at depth, they may still enhance fluid flow in rocks with almost no matrix permeability (Zoback, 2007), and their importance should be evaluated.

**Model of joints.** Examination of lithofacies that are prone to fracture development (i.e., brittle) is easier in outcrop analogs than in subsurface well logs because fractures along bedding planes can be observed. One key observation in the outcrop of Figure 2 is that not all units develop fractures with the same intensity, and some do not fracture at all unless they are near or within a fault zone. In this study, we used careful characterization of an outcrop of the formation of interest by Ferrill et al. (2014)

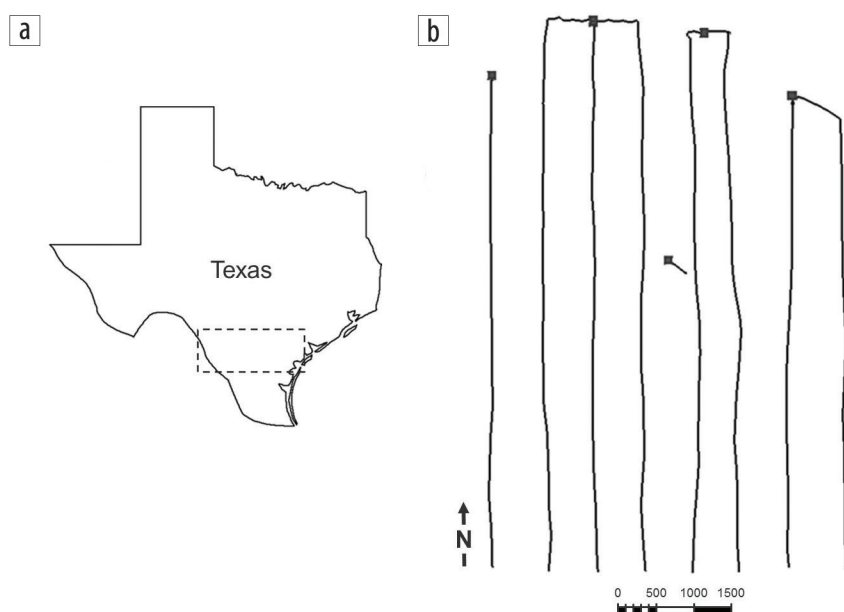


**Figure 1.** (a) Approximate location of the study area (dashed rectangle). (b) Relative locations of wells used in this study: one vertical pilot well near the middle and eight horizontal wells in its vicinity. The area of interest for flow simulation around these wells is approximately 3.6 mi<sup>2</sup>. The scale is in feet. Lateral sections range between 6000 and 7300 ft.

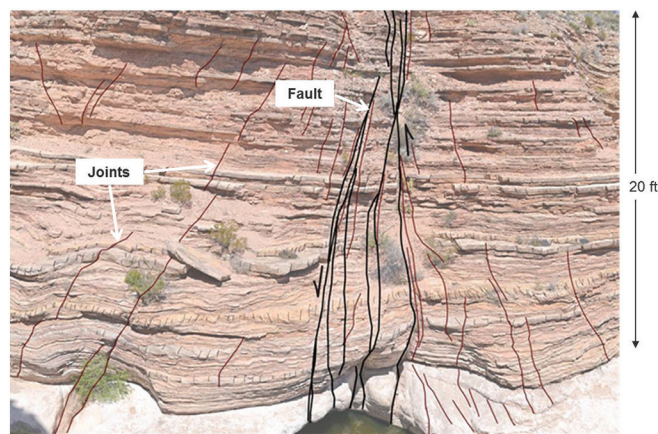


**Figure 2.** Interpreted natural fractures in an outcrop of the Boquillas Formation, which is an analog to the unconventional reservoir analyzed in this study. Joints and faults are marked separately.

that highlights the importance of clay content in the determination of brittle versus nonbrittle facies and therefore the likelihood of fracture development.

Since mechanical rock properties control the distribution of joints, we first perform mechanical facies modeling constrained by facies probabilities derived from prestack inversion results (Michelena et al., 2017). By using mechanical facies that are more or less brittle, we account for the bed-bound nature of the joints whose growth is controlled by mechanical properties. Different facies are assigned different fracture intensities. These intensities are weighted by distance to fault functions that vary by facies to account for the observed mechanically dependent fracture intensity decrease away from faults (Caine et al., 1996). Parameters such as fracture height, fracture length, and fracture aperture are also used. These parameters are extracted from

outcrop, other analogs (Ferrill et al., 2014), and log information.

Strain derived from seismic dip attribute is also used to weight the relative intensities of joints across the area of interest by assigning higher intensities to areas of higher dip. The result is a model for joints that (statistically) honors the well data in terms of intensity and layer thickness and shows the expected behavior with respect to strain and distance to faults.

**Model of small faults.** Through-going fractures are controlled by the presence and proximity of seismic and subseismic scale faults along with mechanical properties of stratigraphic intervals (rather than individual beds). They tend to show significantly higher permeability than joints and may enhance vertical communication between reservoir compartments with different rock properties as shown in Figure 2. After careful calibration with independent fracture data, we selected the maximum curvature as a proxy to model the through-going fractures in this study. Three attribute volumes were extracted from the maximum curvature using the workflow described in Michelena et al. (2013): dominant local strike, Fisher coefficient, and intensity. The extraction of these fracture-related attributes is data driven, and no assumptions are made about any particular fracture geometry or elastic symmetry. Strike orientations are used to separate fracture families that are assigned different properties in the flow simulator to better calibrate with production data. We also assume that the orientations of small faults and joints share the same statistics — a hypothesis that will be confirmed in the next section.

**Fracture quality.** After we model the two different fracture scales with their corresponding geometries and spatial distributions, we estimate their quality (i.e., conductive or nonconductive) based on their relative orientation with respect to the current earth stress state and assessment of any diagenetic process that may have altered the initial void space between fracture surfaces. Often, fractures that are hydraulically conductive are those that are critically stressed in the current stress field (Zoback, 2007). Therefore, besides the origin of the fractures, we used our knowledge of the current stress field to help separate fractures between more and less conductive depending (mostly) on their relative orientation with respect to the maximum horizontal stress. As explained later, dynamic well tests are used in this step to calibrate effective permeabilities.

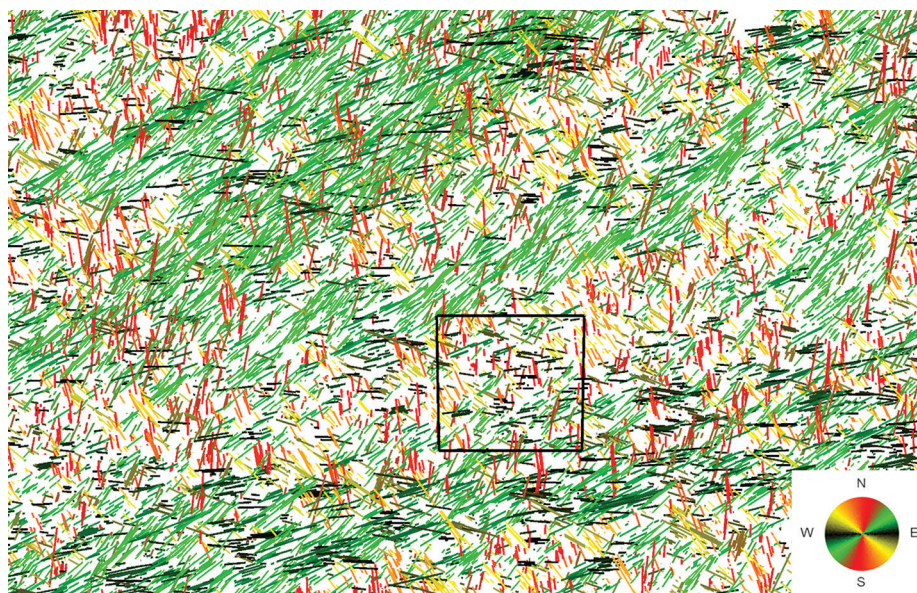


**Figure 3.** Detail of local strike orientations in an area of 280 mi<sup>2</sup>. The area of interest for the simulation study (black) is about 3.6 mi<sup>2</sup>. The dominant orientation is around N45E (green) with a secondary orientation around N45W (yellow). The length of the segments is proportional to the local intensity. Portions of the seismic data are owned or controlled by Seismic Exchange Inc. and Seitel. Interpretation is that of iReservoir.

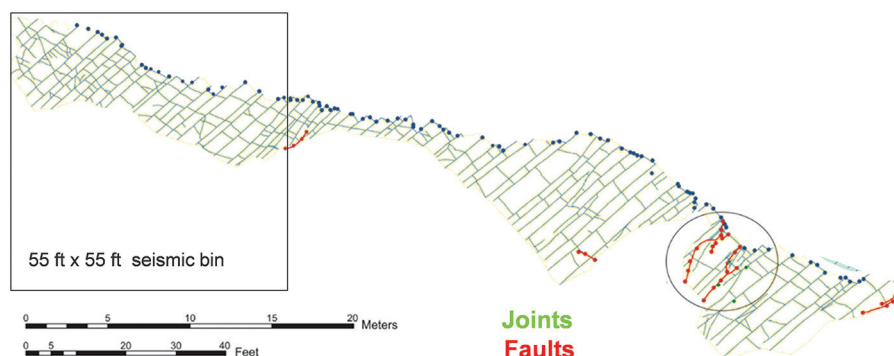


**Figure 4.** Map view of interpreted joints and faults from outcrop (modified from Ferrill et al., 2014). The orientation of the dominant joint set is about N45E and the secondary set is about N45W. Faults (red) show similar orientations. The same two families of orientations are observed at seismic scale (Figure 3). A 55 × 55 ft seismic bin is also shown for comparison of the outcrop and seismic scales. AAPG©2014, reprinted by permission of AAPG whose permission is required for further use.

### Calibration of seismic-derived fracture attributes

As mentioned in the previous section, maximum curvature was extracted from the 3D seismic data and used to extract the local strike orientations shown in Figure 3. These orientations were statistically analyzed in 11 × 11 superbins resulting in local intensities, dominant strike orientations, and Fisher coefficient. The process to estimate intensities and to separate families of fractures is similar to how fracture intensities and families are estimated by counting angles from image log data. As Figure 3 shows, two main families of orientations (green and yellow) can be identified from the seismic data, both in the 280 mi<sup>2</sup> large seismic area and the 3.6 mi<sup>2</sup> area of interest.

Before the statistics of strikes from seismic data can be used to constrain the model of natural fractures, we must check whether these orientations are related to the orientations of actual natural fractures in the area. As Figure 4 from Ferrill et al. (2014) shows,

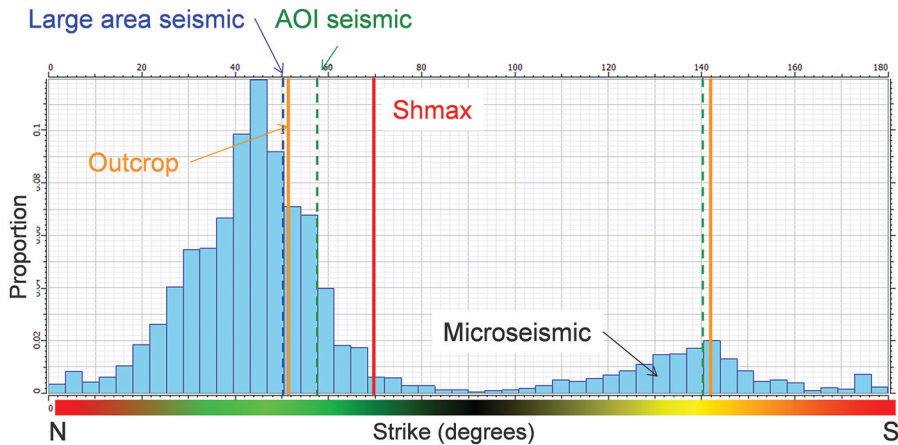


**Figure 5.** Histogram of fracture orientations from microseismic data. Dominant orientations extracted from outcrop, large 3D seismic area, and smaller area of interest are posted for comparison. The same families of orientations are observed at all scales. The orientation of the maximum horizontal stress  $S_{Hmax}$  is also shown in this figure.

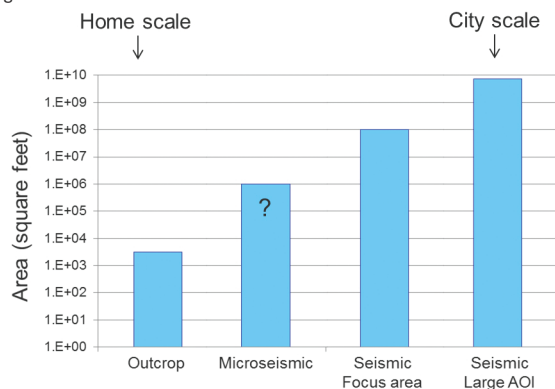


**Figure 6.** Different scales of analysis for orientation of natural fractures. The same two families of orientations are observed across these scales that span approximately seven orders of magnitude. The area covered by the microseismic data is uncertain but is smaller than the area of the simulation model and larger than the area of the outcrop.

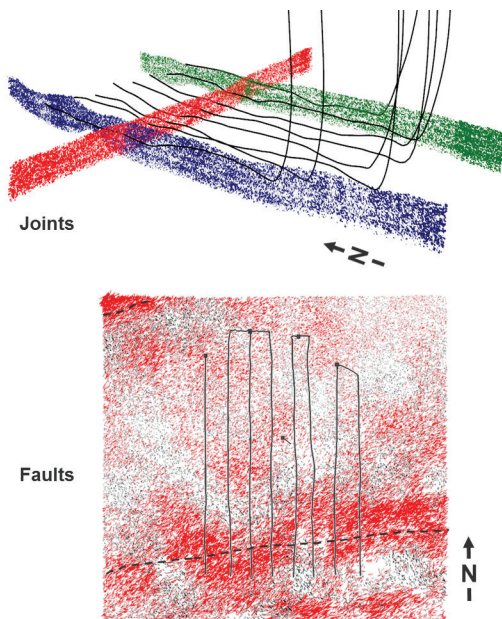


**Figure 7.** Discrete fracture models for joints and faults. Two families of orientations are modeled for each type of fracture. Red and black fault segments indicate dominant and secondary families, respectively. Vertical variability in intensity of joints is related to changes in rock properties. Notice how distance to large faults (dashed lines) also affects the intensity of joints and faults.

two distinctive families of joints are observed in the outcrop. Notice that their orientations and relative intensities coincide with the families of fault orientations derived from seismic data (Figure 3). The few small faults interpreted in the outcrop shown in Figure 4 (in red) also follow the same orientations as the joints. The area covered by the outcrop is a few thousand square feet.

Microseismic data from a surface array related to five of the horizontal wells shown in Figure 1b were also available in this area. A histogram of the orientations of microseismic events from moment tensor inversion is shown in Figure 5. Notice that microseismic-derived orientations also show the same two families of fractures observed in the outcrop, the large seismic area, and the area of interest. Figure 6 compares the different scales of analysis in more detail. The same two families of orientations are observed across all of them. This invariance of orientations across almost seven orders of magnitude confirms that seismic-derived orientations are indeed related to the orientations of actual fractures and therefore are adequate to constrain small-scale fracture models in the area of interest for both joints and small faults.

Figure 5 also shows the orientation of maximum horizontal stress in this area, which is approximately 25° clockwise from the dominant fracture orientation (green family). This suggests that natural fractures along the dominant orientation may be critically stressed (Zoback, 2007) and therefore may exhibit (depending on pore pressure) enhanced flow properties relative to other fracture orientations.

### Discrete fracture network modeling

After the calibration of seismic-derived fracture attributes is complete, we end up with 13 continuous 3D volumes that serve as input for discrete fracture modeling. These volumes contain information about orientation, intensity, and Fisher coefficient for two families of joints and two families of faults. We also exported an additional volume with the global (family-independent) Fisher coefficient per cell.

Figure 7 shows the discrete fracture models for joints and faults that resulted from this workflow. Notice the vertical variability in intensity of joints due to vertical changes in rock properties. Lateral variability in intensity and length of faults is also affected by proximity of faults.

Before these models can be used for flow simulation, they must be upscaled and transformed back into continuum models that the flow simulator can read. As an alternative to discrete fracture models, continuous fracture models (CFM) can also be built directly from the input attributes. CFMs can help achieve a first-pass understanding of the effect of the fractures in the production.

### Fracture properties in the simulator

Three important parameters describe the distribution of fracture properties in the flow simulation model: fracture porosity, effective fracture permeability tensor, and fracture intensity. Performance is significantly impacted by the variability of these three parameters throughout the drainage area.

*Fracture porosity* ( $\phi_f$ ) is generally a very low value compared to matrix porosity and cannot be easily resolved by flow performance because of significant matrix-fracture fluid transfer. Porosity is usually estimated from cores and heuristic arguments. Not all cells in our models have fractures, but for those cells containing fractures, average fracture porosity was about 0.002%. This is much smaller than the average matrix porosity of about 6% for the interval of interest. This very low value of fracture porosity can result in rapid pressure response over long distances. Pressure diffusivity is proportional to  $(k/\phi_f)^{1/2}$  where  $k$  is the fracture permeability. Even for the low average natural fracture permeability noted later, pressure diffusivity is orders of magnitude larger in fractures compared to the joint enhanced matrix permeabilities. Pressure response can be created at large distances through the fractures. However, the magnitude of this pressure response through the fractures is limited by the large fracture matrix surface area as noted later.

*Fracture network effective permeability* is highly directional and stress dependent because of preferred fracture orientations and

the stress dependency of aperture. As we will explain later, the estimation of this anisotropy requires estimates of fracture orientations and present-day stress calibrated to well productivity. Natural fracture permeability distribution is also highly variable. As shown in Figure 7, faulted areas have more intense fracturing, which will lead to more pressure interference along the fault.

*Fracture intensity* is a measure of matrix-fracture contact surface area that allows significant fluid transfer from the low-permeability matrix into the fracture. Estimating effective fracture intensity was a major effort of this modeling study. When fracture intensity is reduced, HF surface area and stimulated rock volumes (SRVs) must be increased to match historical data. Average fracture intensity (or surface area of the fractures per unit volume) is on the order of  $1 \text{ ft}^2/\text{ft}^3$ .

HF and SRV parameters also represent major history match variables but are constrained by fracture design parameters.

### Model upscaling and effective permeability

The natural fracture models shown in Figure 7 were upscaled for flow simulation using the Oda equation (Oda, 1985). The Oda equation indicates that the effective fracture permeability tensor in a cell is proportional to the sum of the product of individual fracture permeabilities, fracture porosity, and a geometric factor related to the (seismic-derived) fracture orientations as follows:

$$k_{eij} \propto \sum_{k=1}^{N_f} \left( \frac{w_f^2}{12} \right)_k \left( \frac{w_f A_f}{\Delta x \Delta y \Delta z} \right)_k (n_i n_j)_k, \quad (1)$$

where  $k_{eij}$  is the effective permeability in a cell that is crossed by  $N_f$  fractures,  $w_f$  is the fracture width,  $A_f$  is the fracture area,  $\Delta x \Delta y \Delta z$  is the cell volume, and  $n_i$  is the projection of the normal to the

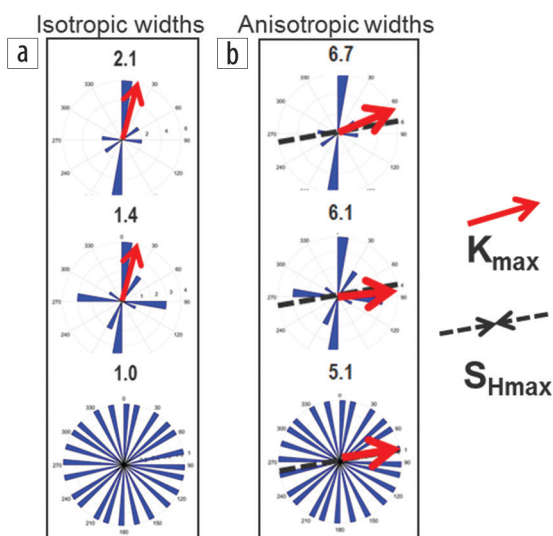


**Figure 8.** Rose diagrams of different scenarios of families of open vertical fractures. (a) Orientation of maximum horizontal permeability  $K_{max}$  (red) assuming an isotropic aperture distribution. (b) Orientation of effective  $K_{max}$  assuming an anisotropic aperture distribution (0.3 mm for critically stressed fractures, 0.2 mm for fractures parallel to  $S_{Hmax}$  and 0.1 mm for nonconductive fractures). Numbers above each rose diagram indicate the corresponding permeability anisotropy  $K_{max}/K_{min}$ . All fractures are open, but their contribution to flow may be significantly different. Isotropic fracture distributions may yield highly anisotropic flow when stress is considered.

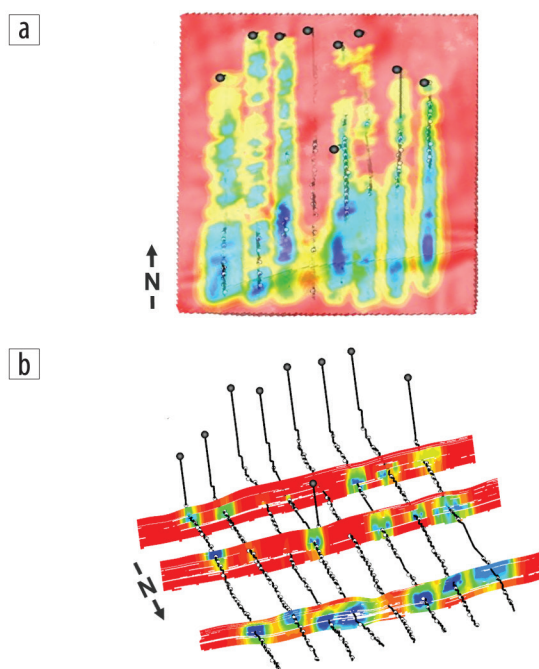


**Figure 9.** (a) Plan view of the average pressure field around horizontal wells in the reservoir estimated from dual-permeability flow simulation after history matching. Red represents initial pressures. (b) Vertical pressure depletion showing heterogeneous behavior.

fracture  $k$  along the  $i^{\text{th}}$  axis. Notice that the effective permeability is proportional to the cube of the fracture width  $w_f$  of the individual fractures (a relation also known as cubic law). In cases when joint width is also proportional to fracture length, effective permeabilities are found to be proportional to width to the fifth power (Klimczak et al., 2010). These types of relations result in  $w_f$  playing a dominant role in determining which fracture has a larger contribution to the overall effective permeability when a cell is crossed by several natural fractures. Fracture width, in turn, depends on current stress state and diagenetic alterations that may have filled the initial void space.

By assuming a small fracture porosity as mentioned earlier, equation 1 can be calibrated with dynamic well test data to estimate a hydraulic aperture for conductive fractures. Two observations wells (one vertical and one horizontal) along with response between offset wells during rate changes or shut-in periods help to calibrate the effective fracture properties in equation 1. Equation 1 can be considered an integration equation because it relates in single expression engineering measurements, geologic fracture properties, geomechanics effects on aperture, and seismic-derived geometric information.

To better understand the relationship between effective permeability and stress implied by equation 1, we modeled the effect of stress by changing the fracture width with respect to the angle between  $S_{H_{\text{max}}}$  and each fracture strike for different fracture geometries. Figure 8a shows the orientation of the maximum permeability  $K_{\text{max}}$  (determined from the effective permeability tensor) when equal fracture widths are used for all fracture orientations to simulate an isotropic stress field. In this case, the orientation of  $K_{\text{max}}$  coincides with the orientations of the most intense fractures. Figure 8b shows the result of assuming an anisotropic aperture function that enhances the fracture permeability for critically stressed fractures compared to other orientations. In this case, the orientation of  $K_{\text{max}}$  is closer to the fractures with wider apertures (critically stressed) even if they are less intense. Due to the cubic law, the wide critically stressed fractures in this example are 27 ( $3^3$ ) times more conductive than the thin ones, which explains the disproportional contribution of the less intense fractures into the effective flow. For this reason, and since the widths of joints are expected to be smaller than the widths of critically stressed faults, the contribution of joints to the effective fracture permeability was also considered small. We added their contribution to the matrix permeability to create a fracture enhanced matrix. The final matrix permeability preserves the variation of joint permeability as well as that of the matrix. Only small faults were included in the final fracture model for calibration with dynamic data.

### Flow simulation

The purpose of the simulation was to develop an integrated view of the reservoir for the purpose of understanding possible well interference, its impact on long-term recovery, and optimal well spacing. While history matching is one aspect of this study, history matching as a standalone task is nonunique. For example, rate-transient analysis of the wells provides one model of the reservoir that suggests relatively short effective HF's (< 200 ft). However, that is not entirely consistent with rapid pressure communication seen between wells. In addition to individual well flowing tubing head pressure (converted to bottom hole pressure),

the model was constrained to the pressure responses of two observation wells (the vertical pilot well and one horizontal).

The fracture models described earlier were combined with a previously generated model for matrix porosity and permeability (Michelena et al., 2017) to define detailed heterogeneous permeability and porosity fields in a dual-permeability simulator. Fine gridding throughout the drainage area of a seven-well development was required to capture the important matrix, natural fracture, and stimulated fracture heterogeneity, which results in complex long-term pressure depletion. Fine gridding near the wells as a common method of LGR is not sufficient for understanding long-term interference. It is important to track long-term pressure depletion throughout the area of interest as well as short-term transients. For this eight-well drill spacing unit, the model was approximately 1.2 million active cells. Cell dimensions were on the order of  $50 \times 50 \times 4$  ft. With these grid sizes, the use of dual permeability with small porosity in the fractures not only behaves similar to an LGR for early time pressure response modeling but also allows long-term tracking of pressure change over large distances. This large detailed grid system with very low effective fracture permeability was efficiently solved with a GPU-based simulator (Mukundakrishnan et al., 2015). For this three-phase gas condensate with small time steps over a three-year history period followed by a 10-year forecast, simulation runs required only a few minutes, allowing many sensitivity iterations.

As described by Dusseault et al. (2011), fluid and/or proppant injection into a reservoir zone creates new fractures as well as close, shear, or reopen existing cemented fractures. These failure mechanisms may lead to a large microseismic cloud surrounding the area of injected fluids thereby improving reservoir drainage. The heterogeneity of the existing and stimulated fracture network (along with variability in matrix properties) can lead to complex drainage patterns that can promote pressure interference between wells as explained in the next section.

### Summary of flow simulation results

Dual permeability accounts for differences in pressure between matrix and fractures and can explain rapid pressure communication between wells and observations points. For this work, pressures from the vertical observation well and a shut-in horizontal well were available to calibrate dual-permeability characteristics that are consistent with the geologic and seismic observations. We observe the following behaviors (also observed in other tight reservoirs) that can be effectively described by the dual-permeability system.

- Apparent permeability from diagnostic fracture injection testing (DFIT) and performance indicate that the permeability from DFIT ( $k_{\text{DFIT}}$ ) is larger than matrix permeability ( $k_M$ ) from core, which suggests a natural fracture contribution to permeability prior to stimulation.
- Although the matrix permeability used for history matching preserves the variation of permeability of the joints as well as that of the matrix, it is smaller than both from a magnitude standpoint. The average enhanced matrix permeability had to be lowered (up to about 60 nanodarcies) to the extent that we no longer observed pressure recharge. To achieve this pressure recharge free model, permeabilities of small widely spaced faults

(the natural fractures in our model) cannot be increased too much. Fracture network permeability varies from zero for cells with no fractures to 30 microdarcies near the fault. Most values are in the range of 220 to 1226 nanodarcies.

- Propped and enhanced permeability regions in the SRV are required to match well productivity. The SRV results from shearing of existing natural fractures to create enhanced apertures. This provides a large surface area to allow low-permeability matrix to be effectively depleted ( $k_{\text{PROPPED}} > k_{\text{SRV}} > k_{\text{DFIT}} > k_{\text{M}}$ ).
- Well productivity declines with time as a result of significant hydraulic and natural fracture compaction.
- Many of the propped and open natural fractures are water filled during stimulation and may be super charged after stimulation. In addition, some treatment fluid may be forced into the matrix next to the stimulated areas as well as moved large distances from the wells where low velocity in the fractures and compaction limit effective cleanup. These characteristics allow the dual-permeability model to match the long-term water rate decline and incomplete flowback of treatment fluids.

Two- and three-phase flow in this area is complex, which is typical of naturally fractured systems. The modeled system in this study is a gas condensate. Dew point pressure is nearly 60% lower than initial reservoir pressure. We observe that well condensate production drops quickly to yield one-half the laboratory values in a very short period. The low pressure (below dew point) established throughout the near-well connected fractures allows the producing yield to stabilize as an oil saturation is quickly established in the matrix next to the fractures, slowing feed into the fracture network.

Figure 9a shows end of history matching pressure averaged over all the simulation layers and illustrates how the natural fracture description and calibration to dynamic well data leads to very complex pressure depletion. Heterogeneity of pressure depletion is apparent at the end of the history match period because of matrix and natural fracture heterogeneity as affected by stimulation. The southern more fractured area near a large fault shows very high depletion (blue), and the red color shows large areas that have not been effectively drained. Depletion in the northern area increases from east to west suggesting that optimal well spacing may vary even in small areas like this due to the complexity of the naturally fractured system. Vertical pressure depletion also reflects heterogeneous behavior as shown in Figure 9b. The average propped height of 50 ft is impacted by mechanical barriers (typically in the form of more ductile layers) over the 107 ft reservoir height.

## Conclusions

We have presented a seismic constrained geologic modeling workflow in naturally fractured reservoirs that considers the geologic, geomechanic, and dynamic parameters that control fluid flow. Calibration with well test and pressure information is important to increase confidence in the results. The pressure field that results after performing flow simulation using this seismically constrained model is significantly heterogeneous, impacting long-term well interference and recovery factors and suggesting a spatially varying optimal well spacing that is different from that defined via the common assumption of homogeneous low matrix permeability and uniform HFs. ■■

## Acknowledgments

We thank BHP Petroleum for permission to publish these results and Mauricio Florez for his support during this project. We also thank Liwei Cheng for his help in estimating Kmax with the Oda equation.

## Data and materials availability

Data associated with this research are confidential and cannot be released.

Corresponding author: michelena@ireservoir.com

## References

- Caine, J. S., J. P. Evans, and C. B. Forster, 1996, Fault zone architecture and permeability structure: *Geology*, **24**, no. 11, 1025–1028, [https://doi.org/10.1130/0091-7613\(1996\)024<1025:FZAAPS>2.3.CO;2](https://doi.org/10.1130/0091-7613(1996)024<1025:FZAAPS>2.3.CO;2).
- Cipolla, C. L., T. Fitzpatrick, M. J. Williams, and U. K. Ganguly, 2011, Seismic-to-simulation for unconventional reservoir development: SPE, Extended Abstracts, <https://doi.org/10.2118/146876-MS>.
- Dusseault, M., J. McLennan, and S. Jiang, 2011, Massive multi-stage hydraulic fracturing for oil and gas recovery from low mobility reservoirs in China: *Petroleum Drilling Techniques*, **39**, 6–16.
- Farah, N., 2016, Flow modelling in low permeability unconventional reservoirs: Ph.D. thesis, Université Pierre et Marie Curie.
- Ferrill, D. A., R. N. McGinnis, A. P. Morris, K. J. Smart, Z. T. Sickmann, M. Bentz, D. Lehrmann, and M. A. Evans, 2014, Control of mechanical stratigraphy on bed-restricted jointing and normal faulting: Eagle Ford Formation, south-central Texas: *AAPG Bulletin*, **98**, no. 11, 2477–2506, <https://doi.org/10.1306/08191414053>.
- Klimczak, C., R. A. Schultz, R. Parashar, and D. M. Reeves, 2010, Cubic law with aperture-length correlation: Implications for network scale fluid flow: *Hydrogeology Journal*, **18**, no. 4, 851–862, <https://doi.org/10.1007/s10040-009-0572-6>.
- Michelena, R. J., K. S. Godbey, H. Wang, J. R. Gilman, and C. K. Zahm, 2013, Estimation of dispersion in orientations of natural fractures from seismic data: Application to DFN modeling and flow simulation: *The Leading Edge*, **32**, no. 12, 1502–1512, <https://doi.org/10.1190/tle32121502.1>.
- Michelena, R. J., K. S. Godbey, and O. G. Angola, 2017, Integrated facies modeling in unconventional reservoirs using a frequentist approach: Example from a South Texas field: *Geophysics*, **82**, no. 6, B219–B230, <https://doi.org/10.1190/geo2017-0041.1>.
- Mukundakrishnan, K., K. Esler, D. Dembeck, V. Natoli, J. Shumway, Y. Zhang, J. Gilman, and H. Meng, 2015, Accelerating tight reservoir workflows with GPUs: SPE, Extended Abstracts, <https://doi.org/10.2118/173246-MS>.
- National Research Council, 1996, Rock fractures and fluid flow: Contemporary understanding and applications: The National Academies Press.
- Oda, M., 1985, Permeability tensor for discontinuous rock masses: *Geotechnique*, **35**, no. 4, 483–495, <https://doi.org/10.1680/geot.1985.35.4.483>.
- Torres-Parada, E. J., S. Sinha, L. E. Infante-Paez, R. M. Slatt, and K. J. Marfurt, 2018, Seismic to simulation: Woodford Shale case study in Oklahoma, USA: URTEC, Extended Abstracts, 1135–1151, <https://doi.org/10.15530/urtec-2018-2886614>.
- Yan, B., J. E. Killough, Y. Wang, and Y. Cao, 2013, Novel approaches for the simulation of unconventional reservoirs: URTEC, Extended Abstracts, 1304–1313, <https://doi.org/10.1190/urtec2013-131>.
- Zoback, M. D., 2007, Reservoir geomechanics: Cambridge University Press.